Optimality

www.opt.reapress.com

Opt. Vol. 3, No. 3 (2026) 248–269.

Paper Type: Original Article

Distributed Influence Search for Engineering Optimization: Conditional Analysis and Reported Benchmarks

Bilal Ahmad Khan[1,*], Wolfgang H. Müller[2]

[1] Department of Computer Science, COMSATS University Islamabad, Islamabad, Pakistan; bilal.khan@comsats.edu.pk.
[2] Department of Computer Science, Technical University of Munich, Munich, Germany; bilal.khan@comsats.edu.pk.

Citation:

Received: 12 April 2026 *Revised: 27 June 2026* *Accepted: 12 August 2026*	Khan, B. A., & Müller, W. H. (2026). Distributed influence search for engineering optimization: Conditional analysis and reported benchmarks. *Optimality, 3*(3), 248-269.

Abstract

Distributed Influence Search (DIS) uses fitness-gated movement on a periodically rebuilt nearest-neighbor graph, a feedback rate based on fitness-weight entropy, and stagnation-triggered recovery. This paper specifies those mechanisms for constrained continuous search and separates them from the assumptions needed for convergence. A valid coverage argument requires a fixed objective, consistently evaluated elitist memory and a uniform conditional probability of reaching relevant sublevel sets; unbounded Gaussian and Cauchy proposals with ε-level acceptance do not establish these conditions by themselves. Reported benchmark, ablation and application summaries are retained for descriptive analysis. They show lower DIS means on several displayed function rows, a 40-dimensional advantage for L-SHADE in the reported rank summary, and different leaders across engineering tasks. Their inferential interpretation remains limited by unresolved evaluation counts, run-level outputs, interval calculations and application feasibility definitions. The 40- and 80-dimensional benchmark settings extend the official CEC 2022 dimensional protocol. The study therefore presents a conditional analysis and a corrected account of reported observations, without certifying global convergence, matched computational work or deployment feasibility.

Keywords: Distributed influence search, Information diffusion, Metaheuristic optimization, Constrained continuous optimization, Swarm intelligence, Engineering design.

1 | Introduction

Engineering optimization can combine nonconvex objectives, nonlinear constraints and expensive evaluations. Economic dispatch includes power balance and generator bounds, with valve-point effects creating nonsmooth cost curves [1], [2]. Robot motion planning must account for configuration-space obstacles and, for dynamic systems, admissible trajectories [3], [4–6]. Population search offers candidate-

Corresponding Author: bilal.khan@comsats.edu.pk
https://doi.org/10.22105/opt.v3i3.118
Licensee System Analytics. This article is an open access article distributed under the terms and conditions of the Creative Commons Attribution (CC BY) license (http://creativecommons.org/licenses/by/4.0).

generation mechanisms for these settings, but gradient-based methods remain useful when derivatives, suitable relaxations or problem structure are available. genetic algorithms (GAs), Particle Swarm Optimization (PSO), Differential Evolution (DE), CMA-ES, SHADE and L-SHADE provide different representations and feedback mechanisms [7-9]. Interaction topology and parameter control vary within these families. This paper does not assume that their interactions are universally static or that network adaptation is absent from established optimization. Network models offer a vocabulary for locality and transmission. Small-world networks, compartmental epidemic models and heterogeneous contact structures describe different spreading phenomena [10-12]. Their results depend on specified dynamics and graph limits; an optimization metaphor does not inherit their epidemic thresholds or convergence properties automatically. The design question here is how fitness-gated transfers on a changing local graph affect population search. The no-free-lunch theorem concerns averages over defined problem classes [13], rather than a mandate for a particular adaptive architecture. Constraint-handling research likewise provides several useful comparison rules whose performance depends on the problem and implementation [14], [19–21].

Three questions guide the analysis: How the reported accuracy compares with the displayed baselines; what configuration differences appear in the ablation; and how the reported engineering and dynamic-environment outcomes depend on feasibility and evaluation conventions. The original records needed to test these questions are distinguished from the summary observations retained here. At the level of specification, Distributed Influence Search (DIS) couples a directed nearest-neighbor graph with a gated centroid move, fitness-weight entropy feedback, Gaussian drift and Cauchy recovery. The graph and schedules are explicit; some boundary, archive, normalization and evaluation-counter choices remain unresolved. The conditional mathematical analysis concerns a fixed penalized objective and a hypothetical archive evaluated under that same objective. It establishes a coverage proposition when the proposal and archive assumptions hold. It does not certify those assumptions for *Algorithm 1* as reported.

The empirical material comprises benchmark point summaries, ablations, threshold counts, application metrics and moving-peaks summaries. Original numerical table entries and plots are retained. The missing original code and run-level outputs prevent independent computational verification, causal component attribution and confirmation of the claimed inferential protocol. The reported 28.7% and −6.8% accuracy aggregates require a complete function-by-method record and an explicit zero-error convention. They are not verified strongest-baseline-per-function effects from the abbreviated table. The displayed data support narrower arithmetic comparisons discussed in Section 6. The influence-removal configuration has the largest displayed ablation gap. That contrast concerns the entire declared removal, including its gate and directional move; it does not identify a separable causal percentage contributed by influence.

Formation error, dispatch cost and dynamic tracking are separate outcomes. Their reported differences cannot establish practical feasibility or robustness without the original instance definitions, tolerance rules, scenario pairing and evaluation traces. The contribution is a specified influence-based search architecture, a conditional coverage analysis, and a calibrated interpretation of the reported summaries. Novelty and comparative performance are limited to these statements; no claim of the first adaptive network optimizer or universally superior operator semantics is made. Fitness-weight entropy measures concentration of selection weights. It is used to regulate transmissibility, while an independent time schedule regulates recovery. Neither quantity directly measures geometric population diversity or implements an epidemiological reproduction number. Penalty scoring gates influence, whereas ε-level comparison governs ordinary acceptance. These criteria can order candidates differently. Their interaction is explicitly addressed in Sections 3 and 4. The complexity analysis separates movement, objective and constraint evaluation, and graph maintenance. A nearest-neighbor index does not supply a dimension-independent logarithmic query guarantee.

The described static protocol uses 41 runs per function and fourteen comparator methods. The official CEC 2022 report defines 10- and 20-dimensional tests, so the reported 40- and 80-dimensional settings are extensions whose shift and rotation definitions require the original manifest. Application summaries are interpreted as reported computational studies rather than certified deployments. They identify different

leading methods across tasks, with original instance and feasibility evidence still required. Section 2 reviews the relevant optimization and network mechanisms. Section 3 specifies DIS, Section 4 states conditional coverage and cost results, and Sections 5 and 6 describe and interpret the reported summaries. Section 7 identifies computational and statistical limitations before the conclusions in Section 8.

2 | Background and Motivation

The framework draws on constrained optimization, network transmission and adaptive search. The literature provides design context; it does not validate the implemented DIS schedules or the retained experimental outcomes.

2.1 | Constrained Continuous Optimization in Engineering Practice

The formal object under audit is constrained continuous minimization, stated next.

$$\min_{x\in\mathcal{X}} f(x)\ \text{s.t.}\ g_j(x)\le 0, j=1,\dots,m, h_r(x)=0, r=1,\dots,q. \quad (1)$$

Here X is a closed bounded box in Euclidean space, and f, g_j and h_r describe the objective, inequality constraints and equality constraints. Continuity and a nonempty feasible set provide an existence statement on compact X. Nonconvexity can complicate both local and population search; it does not make gradient projection categorically unreliable. One ubiquitous engineering shortcut folds the constraints into the objective through a penalty multiplier and thereby replaces (1) with the penalized surrogate:

$$F\left(x,\lambda^{(t)}\right)=f(x)+\lambda^{(t)}v(x), v(x)=\sum_{j=1}^{m}\max\left(0,g_j(x)\right)+\sum_{r=1}^{q}|h_r(x)|. \quad (2)$$

In *Eq. (2)*, ν aggregates the displayed general-constraint residuals. It omits box violations. If candidates are allowed outside X, a complete wrapper must also include ν_box(x) = Σ_r[max(0,l_r − x_r) + max(0,x_r − u_r)] or apply an explicitly declared domain rule. Residuals with different physical units require normalization. Penalty and feasibility-first methods provide alternative comparison conventions [14–17], rather than a universally superior single rule. The intended requirements are explicit constraint accounting, feedback responsive to recorded information and a measured computational cost. Each requirement needs an implementation and evaluation ledger. Constraint accounting should include domain bounds, inequalities, equality tolerances and any discrete-variable encoding. A penalty score alone is insufficient to certify a feasible returned solution. Feedback should state the observable that it uses and the proposal parameter that it changes. A fitness-weight entropy signal can be useful even though it does not measure spatial diversity. Cost should include graph queries, candidate evaluations, recovery and archive reevaluation. A simple arithmetic movement bound does not establish end-to-end scalability. These requirements guide the analysis without excluding other feasible optimizer designs. The same criterion must be applied to every compared implementation when a controlled method comparison is claimed.

2.2 | Information Diffusion and Influence Propagation in Network Science

Kermack–McKendrick models, small-world networks and scale-free spreading analyses describe distinct transmission processes [13–15]. Other network models characterize epidemic connectivity and heterogeneous degree distributions [17], [18]. They motivate a local transfer mechanism here, but no epidemic-threshold theorem is derived for the adaptive fitness-gated graph. Threshold adoption, word-of-mouth diffusion, diffusion of innovations and influence maximization offer additional perspectives on information transfer [23–26]. DIS uses a particular fitness-gap gate; these references do not identify it as an empirically validated social or epidemiological process.

DeGroot's consensus model concerns weighted averaging under conditions on its transition structure [26]. The infected-agent centroid in DIS resembles a local average, but changing weights, directed neighborhoods,

acceptance, noise and recovery prevent the consensus theorem from being transferred without a separate analysis. The terminology 'infection' refers to a successful gated transfer, and 'recovery' to a stagnation-triggered reset. Penalized fitness supplies the transfer score. The schedules below define these operations mathematically; β_t times a mean degree is a heuristic transmission summary, not a certified basic reproduction number or proof of self-extinction.

2.3 | Positioning Relative to Existing Metaheuristics

Table 1 summarizes representative mechanisms [27–36]. It does not establish a universal topology, convergence guarantee or scaling range for every variant of each family. Comparisons between a particular implementation and DIS require declared versions and evaluation conventions. Adaptive pursuit, dynamic bandit selection, credit assignment and parameter-control research provide close context [37–40]. DIS adapts its neighbor graph and gate instead of merely choosing an operator label. This design distinction is descriptive; it does not show that such adaptation is absent elsewhere or that the method strictly generalizes those algorithms. The conditional result in Section 4 identifies the proposal and archive conditions needed for global coverage of a fixed objective. Those conditions are stronger than positive noise density at each finite state. The empirical summaries are examined separately, rather than treated as validation of the theorem.

Table 1. Representative search mechanisms and scope of comparison.

Algorithm	Interaction Topology	Operator Semantics	Convergence Guarantee	Constraint Handling	Scalability Evidence
GA [6], [7]	None (panmictic)	Fixed crossover and mutation	Variant- and assumption-dependent	External penalties or repair	Variant- and protocol-dependent
PSO [8]	Static (gbest star or lbest ring)	Velocity attraction to leaders	Variant- and assumption-dependent	External penalties	Variant- and protocol-dependent
DE / SHADE / L-SHADE [9], [11], [12]	None (panmictic)	Fixed difference-based mutation; adaptive F and CR	Variant- and assumption-dependent	External penalty or epsilon-level variants	Source 100D range unverified; protocol-dependent
CMA-ES [10]	None (full covariance model)	Distribution update (self-adaptive)	Variant- and assumption-dependent	External repair or penalty	Source 100D range unverified; protocol-dependent
GWO [30]	Fixed leader hierarchy	Encircling moves toward leaders	Variant- and assumption-dependent	External penalties	Protocol-dependent
WOA/ HHO/ALO [31], [32], [33]	None or implicit	Metaphor-based encirclement and raiding	Variant- and assumption-dependent	External penalties	Source 100D range unverified; protocol-dependent
DIS (this work)	Directed k-NN graph, periodically rebuilt in decision space	Gated centroid, Gaussian drift and Cauchy recovery	Conditional fixed-score archive result (Proposition 1)	Changing penalty and epsilon comparison; feasibility unverified	Source 30-100D range unreconciled; descriptive scaling

Statements about theory and dimension ranges are qualified by the implementation and evidence available; the DIS convergence entry refers to a conditional proposition, not a verified property of the reported run protocol. Rows group algorithms by structural family rather than by chronological order.

3 | The Distributed Influence Search Framework

This section specifies the influence graph, gated centroid move, entropy feedback and recovery schedules. It also identifies missing boundary, evaluation and archive conventions. Candidate positions are denoted x_i, the graph G_t and the feedback rate β_t.

3.1 | Overview: Search as an Epidemic on a Solution Network

An iteration rebuilds the graph when scheduled, rescales current fitness information, draws gated transfer events, proposes local moves and applies ordinary acceptance or recovery. Recovered agents immediately become eligible for later transfer attempts. The epidemic-state terminology does not introduce a separate implemented compartment process beyond these operations. Neighborhoods determine movement, while fitness standard deviation, entropy, objective normalization and archive bookkeeping use population-level information. Thus 'distributed' describes local transfer semantics, not a demonstrated decentralized implementation or a proof that agents require only two globally shared scalars.

3.2 | Dynamic Interaction Topology

The influence graph is a directed k-nearest-neighbor graph built in decision space. Let ϱ^(t)(i, j) denote the rank of agent j among the neighbors of agent i when all other agents are ordered by Euclidean distance from x_i, so that ϱ^(t)(i, j) = 1 identifies the nearest neighbor. The edge set at iteration t is:

$$E^{(t)} = \{(i,j) \in V \times V : \rho^{(t)}(i,j) \leq k\}. \quad (3)$$

Eq. (3) is interpreted literally as a directed proximity graph: (i,j) is present when j is among the k nearest other agents to i. Transmission in *Eq. (4)* then flows i to j when i has a smaller current score. Incoming and outgoing neighbor sets are different; a recipient can have more than k incoming edges. With N > k and a fixed tie rule, the graph has Nk edges and mean in-degree k, but no per-recipient in-degree bound of k follows. The reported settings are k = 5 and a rebuild period R = 5. Distances are measured in decision coordinates, so variable scaling affects neighbor selection. Nearby positions need not have similar objective values on every landscape. Shrinking neighbor distances may shorten centroid moves, but Gaussian drift and Cauchy recovery can still produce large steps. A k-d tree is one possible spatial index [40]. Build and query costs depend on dimension, data distribution and tie handling; exact nearest-neighbor queries can degrade toward a full scan. The original query implementation and runtime breakdown are required before O(N log N/R) can be asserted for all graph maintenance.

3.3 | Influence Propagation Operators

Let a directed edge (i, j) be present in the graph at iteration t. Agent i can transmit influence to agent j only when it is strictly fitter under the penalized objective, F(x_i^(t)) < F(x_j^(t)); transmission then succeeds with probability:

$$p_{i\to j}^{(t)} = \beta^{(t)} \sigma\left(\frac{F\left(x_j^{(t)}\right) - F\left(x_i^{(t)}\right)}{\tau^{(t)}}\right), \sigma(z) = (1 + e^{-z})^{-1}. \quad (4)$$

The transmission formula applies only to present edges whose source is strictly fitter. The temperature is reported as max(10^−8,s_t), with s_t the population score standard deviation. The small floor prevents division by zero but breaks exact scale invariance when it is active. Independent Bernoulli draws must be understood conditionally on the current graph and scores; stable sigmoid evaluation is needed for extreme score gaps. The set I_j contains incoming source agents whose gated transmission to j succeeds. The weighted centroid in *Eq. (5)* is defined only when that set is nonempty. Otherwise no centroid is evaluated and the candidate uses the drift-only branch.

$$\bar{x}_j^{(t)} = \frac{\sum_{i \in I_j^{(t)}} p_{i \to j}^{(t)} x_i^{(t)}}{\sum_{i \in I_j^{(t)}} p_{i \to j}^{(t)}}. \tag{5}$$

For a nonempty successful-infection set, *Eq. (6)* combines the centroid direction with Gaussian drift. All positions and event probabilities should be read from a declared iteration snapshot; sequential updates would define a different transition kernel.

$$x_j^{(t+1)} = x_j^{(t)} + \gamma_j^{(t)} \left(\bar{x}_j^{(t)} - x_j^{(t)} \right) + \eta^{(t)} \xi_j^{(t)}, \gamma_j^{(t)} = \min \left(1, \sum_{i \in I_j^{(t)}} p_{i \to j}^{(t)} \right), \xi_j^{(t)} \sim \mathcal{N}(0, I_d). \tag{6}$$

The recorded schedule $\eta_t = \eta_0(1 - t/T) + \eta_min$ starts at $\eta_0 + \eta_min$ when $t = 0$ and ends at η_min. It does not start at η_0. Gaussian drift has support throughout Euclidean space at every fixed finite state, but the density on X has no uniform lower bound over unbounded possible means. The drift-only branch is used when no infection succeeds. A complete-graph setting still lacks particle velocity memory and is not a strict generalization of gbest PSO. Ordinary acceptance follows *Eq. (13)*. It can accept a candidate with lower violation and a much worse objective, so it need not decrease a fixed penalized score F. Recovery bypasses this comparison. A separate fixed-score archive, if used for the conditional theory, must evaluate every candidate under its own declared criterion. For example, with $\varepsilon = 1$ and $\lambda = 1$, parent $(f,v) = (0,0)$ has $F = 0$, while candidate $(-0.1,0.5)$ is also ε-feasible and is accepted because its objective is lower, although $F = 0.4$. Thus *Eq. (13)* does not imply the fixed-penalty archive property used by the conditional proposition.

3.4 | Exploration–Exploitation Regulation via Diffusion Rate

The feedback loop first maps current penalized scores into Gibbs weights. Stable computation should subtract a common score before exponentiation, which preserves the normalized weights and avoids numerical underflow or overflow.

$$q_i^{(t)} = \frac{\exp\left(-F\left(x_i^{(t)}\right)/\zeta^{(t)}\right)}{\sum_{l=1}^{N} \exp\left(-F\left(x_l^{(t)}\right)/\zeta^{(t)}\right)}. \tag{7}$$

The reported temperature $\zeta_t = \max(10^{-8}, s_t)$ uses the current population score scale. *Eq. (8)* is the Shannon entropy of these weights, not a spatial diversity index.

$$H^{(t)} = -\sum_{i=1}^{N} q_i^{(t)} \ln q_i^{(t)} \in [0, \ln N]. \tag{8}$$

The entropy lies between zero and $\ln N$ for $N > 1$. Equal scores give equal weights, whereas concentration of weights lowers entropy. Spatially distinct agents can have equal scores, and spatially similar agents can have different scores; the two notions of diversity should not be equated.

$$\beta^{(t)} = \beta_0 \left(1 - \frac{H^{(t)}}{\ln N} \right). \tag{9}$$

With $\beta_0 = 0.7$, the recorded feedback rate ranges from zero to β_0. Equal weights suppress gated transfers, while concentrated weights increase their rate. This algebraic property does not establish epidemic takeoff, global exploration or a favorable sequence of optimization phases. Recovery supplies the counterweight to propagation. Agents whose personal best has not improved for $S = 15$ consecutive iterations are declared stagnant and recover with probability:

$$\mu^{(t)} = \mu_{min} + (\mu_{max} - \mu_{min}) \frac{t}{T}. \tag{10}$$

The recovery endpoints are reported as μ_min = 0.05 and μ_max = 0.35, with stagnation span S = 15. A recovering agent is reset through *Eq. (11)*, bypassing ordinary acceptance. The stagnation criterion requires a declared personal-best score and its treatment when the penalty coefficient changes.

$$x_j^{(t+1)} = x_j^{(t)} + c^{(t)}\delta_j^{(t)}, \delta_{j,r}^{(t)} \sim \text{Cauchy}(0,1) \text{ for } r = 1, \dots, d. \quad (11)$$

Componentwise Cauchy increments with a scale described as 10% of box width permit unbounded moves. Positive density at a fixed mean is insufficient for a uniform conditional hitting bound when positions can escape arbitrarily far. Recovery also consumes an evaluation and can worsen the current population state. A separately retained and consistently rescored archive can protect a specified best value; that protection is not automatic under changing λ and ε.

3.5 | Constraint Handling

Influence and Gibbs weighting use a penalty score; ordinary acceptance instead uses objective and effective violation. These criteria need not agree. The exponentially scheduled penalty in *Eq. (12)* is finite over a finite run and does not by itself enforce exact feasibility.

$$\lambda^{(t)} = \lambda_0 \left(\frac{\lambda_f}{\lambda_0}\right)^{t/T}. \quad (12)$$

The reported penalty grows from 1 to 10^6 after objective normalization by an initial-population magnitude median. A zero or very small normalization constant needs an explicit safeguard, and physically distinct residuals require scale definitions. The ε level is reported to decay from mean initial violation to 10^−12; if mean initial violation is zero, the geometric endpoint convention must be specified. *Eq. (13)* uses effective violation max(0, ν − ε).

$$x \preccurlyeq_\varepsilon y \Leftrightarrow \hat{v}(x) < \hat{v}(y) \text{ or } \big(\hat{v}(x) = \hat{v}(y) \wedge f(x) \le f(y)\big). \quad (13)$$

At ε = 0, the lexicographic comparison prioritizes lower violation, then lower objective when violations tie, in the spirit of feasibility-based comparison [16], [17]. Beyond the ε level it prioritizes violation; within the level it prioritizes objective. This property does not imply monotonicity of F or of raw violation: An ε-feasible candidate with a higher raw violation can win on objective. The source states that box residuals enter the wrapper, but *Eq. (2)* does not include them; the explicit domain rule must therefore be checked in the original code. Neither an infector's score nor ordinary acceptance proves that the returned archive satisfies nonlinear constraints. The reported static-penalty ablation also changes boundary handling, so it does not isolate a single feasibility-rule effect.

3.6 | Algorithm Specification Checklist

Algorithm 1 describes one newly evaluated candidate per agent per iteration when recovery replaces the ordinary candidate. Initialization adds N evaluations. Any evaluated-and-discarded proposal, noisy reevaluation, archive refresh or recovery evaluation must also be counted. A fixed seed alone does not guarantee exact reproduction across versions or update order. *Table 2* preserves the recorded defaults, including its 30D/50D labels that conflict with the 20D/40D settings stated in the text. The population-size row labels 30D and 50D, whereas the reported primary study uses 20D and 40D; the original configuration manifest must resolve that discrepancy. Temperatures are computed from population scores. The described separate calibration set and tuning budget remain unverified without the original problem list, tuning outputs and selection record.

Table 2. Recorded parameter roles, explored ranges and defaults. Numerical entries are preserved.

Parameter	Symbol	Role	Range Explored	Default
Population size	N	Number of agents	40-120	60 (30D), 100 (50D)
Neighborhood size	k	Out-degree of the influence graph	3-8	5
Base diffusion rate	beta_0	Maximum transmissibility	0.3-0.9	0.7
Recovery rates	mu_min, mu_max	Endpoints of the linear recovery schedule (10)	0.02-0.08, 0.20-0.50	0.05, 0.35
Rewiring period	R	Iterations between graph rebuilds	1-20	5
Noise scales	eta_0, eta_min	Diffusion-noise scale and its annealed floor (6)	0.01-0.20 of box width	0.05, 10^-6 of box width
Stagnation span	S	Iterations without personal-best improvement before recovery is possible	5-30	15
Penalty bounds	lambda_0, lambda_f	Endpoints of the exponential penalty schedule (12)	0.1-10, 10^4-10^8	1, 10^6
epsilon level bounds	epsilon_0, epsilon_f	Endpoints of the geometric epsilon schedule	mean initial violation, 10^-12	as listed
Recovery step	c^(t)	Scale of the Cauchy recovery increment (11)	0.05-0.20 of box width	0.10 of box width
Sigmoid temperature	tau^(t)	Gradient-gating scale in (4)	adaptive	max(10^-8, std of F)
Selection temperature	zeta^(t)	Gibbs weights in (7)	adaptive	max(10^-8, std of F)

Algorithm 1. Required ordering and evaluation checklist.

1: Input: explicit evaluation budget B, population N, neighbor count k and all recorded schedules.
2: Declare domain handling, normalized residuals, feasibility tolerances and synchronous or sequential update order.
3: Declare archive criteria and every evaluation included in B; do not infer an executed protocol from this checklist.
4: Initialize and evaluate N agents in X; store f and all constraint residuals separately; count these calls.
5: Define penalty scores and operational archives; any fixed-F theoretical archive is separate and explicitly declared.
6: Build the directed graph of Eq. (3), with an explicit distance scaling and tie rule.
7: For each iteration t, continue only while the remaining budget permits the required evaluations.
8: Update λ, ε and η; recompute all comparison scores from stored objective/residual values under the common current coefficient.
9: Rebuild the graph when scheduled; take the declared iteration snapshot before transmission attempts.
10: Compute stable Gibbs weights, their entropy and β from Eqs. (7)–(9).
11: For each recipient j = 1,...,N, stop before a proposal if its evaluation would exhaust the remaining budget.
12: For recipient j, inspect incoming edges (i,j); test strictly fitter sources and draw conditional Bernoulli events.
13: If successful sources exist, form the ordinary candidate from their centroid by Eqs. (5)–(6).
14: Otherwise form the ordinary Gaussian drift-only candidate.
15: End the successful-source condition; no empty centroid denominator is evaluated.
16: If stagnation and the sampled recovery event trigger, select recovery for this recipient.
17: Replace the ordinary candidate by the Cauchy proposal of Eq. (11); do not evaluate both candidates.
18: End the recovery-selection condition.
19: Evaluate the selected proposal once and count that call. Apply the unconditional reset for recovery, or the epsilon comparison for an ordinary proposal; record objective and residuals.
20: Rescore operational archives consistently. A separate theoretical archive retains every eligible proposal in X evaluated under its fixed F, including a proposal rejected operationally.
21: End the recipient loop.
22: End the iteration loop when the stated stopping rule or counted budget is reached.
23: Return the candidate, objective, constraint residuals, declared feasibility result and complete evaluation count.

The pseudocode clarifies the required graph orientation, counter and archive conventions. These reporting repairs do not claim that the completed checklist generated the retained tables. Original source code must identify the actual branches and provide ablation correspondence.

4 | Theoretical Analysis

This section establishes a conditional coverage result for a fixed objective and a separate cost decomposition. It explains why the source assumptions do not follow automatically from unbounded proposals and ε-level acceptance.

4.1 | Conditional Global Coverage

Let F be a fixed continuous penalized objective on compact X, and F* its minimum. Index individual evaluated proposals by s rather than counting a full population iteration as one bounded increment. The following additional conditions define the proposition.

A1: Every relevant δ-sublevel set $X_\delta = \{x \text{ in } X: F(x) \leq F^* + \delta\}$ has positive measure under a declared reference distribution on X.

A2: Conditionally on every reachable history, proposal s hits X_δ with probability at least a fixed $p_\delta > 0$. An independent positive-rate refresh from that reference distribution is one sufficient mechanism. Neither such refresh nor a uniform density bound over unbounded Gaussian/Cauchy means is established for the reported algorithm.

A3: A separate archive B_M stores the minimum exact F value among every eligible proposal in X under the same fixed F. This archive assumption is distinct from epsilon-lexicographic operational acceptance and changing penalty scores; out-of-box candidates are ineligible for this fixed-domain theorem. Under A3, the fixed-score gap potential has the conditional nonincrease property in *Eq. (14)*:

$$\Phi_M = B_M - F^\star \geq 0, \qquad \mathbb{E}[\Phi_{M+1} \mid \mathcal{F}_M] \leq \Phi_M. \tag{14}$$

A bounded-below monotone archive gap converges, but monotonicity alone does not identify its limit as zero [40], [41]. Coverage supplies the missing argument. For completeness, *Eq. (15)* gives a valid proposal-index martingale bound centered by the sum of conditional hit probabilities, rather than by the unconditional expected total count.

Proposition 1. Under A1–A3, $\Pr(B_M - F^* > \delta) \leq (1 - p_\delta)^M$. Thus B_M tends to F* in probability; applying the bound at every positive rational δ also gives almost-sure convergence of the nonincreasing archive gap. The result concerns an unlimited fixed-objective sequence, not the finite changing-score run in *Algorithm 1*.

$$\Pr\left(\left|\sum_{s=1}^{M}(I_s - p_s)\right| \geq a\right) \leq 2\exp\left(-\frac{a^2}{2M}\right). \tag{15}$$

Proof: Let E_s be the event that the first s proposals all miss X_δ. Conditional coverage gives $\Pr(E_s) \leq (1 - p_\delta)\Pr(E_{s-1})$; induction yields the product bound. A hit is retained by A3, independently of whether operational ε-acceptance would accept it. The events of never hitting a fixed X_δ have probability zero. Their countable union over positive rational δ has probability zero, so the archive limit is F*. For *Eq. (15)*, write I_s for the hit indicator and $p_s = E[I_s \mid \text{history before s}]$. The increments $I_s - p_s$ have conditional mean zero and absolute value at most one, so Azuma's inequality applies to their partial sum. No count increment bounded by one is assumed for an entire N-agent iteration.

The proposition is conditional and does not prove global convergence of the reported ε-accepted chain. The changing λ–ε schedule, unrestricted out-of-box states, finite coefficient, noisy scoring and dynamic objectives

require separate arguments. Positive proposal density at each state does not establish a uniform bound over all states. Terminal small errors or an ablation contrast cannot verify these mathematical assumptions [18,42].

4.2 | Computational Complexity

Let C_f and C_ν denote the actual costs of objective and residual evaluation, and C_graph the full rebuild-and-query cost. Gated centroid movement touches Nk edges overall and costs O(Nkd). With one candidate evaluation per agent, *Eq. (16)* separates these terms from graph maintenance amortized across R iterations. Constraint counts alone do not identify evaluation costs.

$$C_{iter} = O\left(Nkd + N(C_f + C_\nu) + \frac{C_{graph}}{R}\right). \quad (16)$$

Memory is O(Nd + Nk) for positions and the sparse graph, plus archives and evaluation records. For fixed k, movement arithmetic is O(Nd). Exact graph queries can approach $O(N^2d)$ work in an unfavorable regime, so the full algorithm is not uniformly linear in dimension. Reported topology overhead, time-to-target and expensive-evaluation percentages require timing and counter traces before they are interpreted as a validated runtime result.

5 | Experimental Design

The reported study addresses static benchmark accuracy, configuration removal, constrained applications and dynamic tracking. Claims that the design, contrast family or fallback was preregistered require a timestamped protocol; no such evidence is supplied with these summaries.

5.1 | Benchmarks and Real-World Problems

The named suite has twelve functions and a known bias convention [41]. The official CEC 2022 dimensions are 10 and 20, with 30 runs and official maximum evaluations of 200,000 and 1,000,000, respectively. Here the described study uses 41 runs and 5,000d evaluations at 20D and 40D, with an 80D extension. These are custom settings, not full official protocol compliance. The exact extension, shifts, rotations, known optima and box wrapper require the original manifest; boundary-interacting optima are not inferred from the suite label. Other CEC collections, including the CEC 2017 suite [42], [43], define different functions and cannot be substituted on the basis of a function label alone. The reported engineering set contains welded-beam, pressure-vessel, speed-reducer and gear-train instances at 25,000 evaluations and 41 runs per method. Canonical versions differ in residual counts and discrete variables. Gear-tooth counts and any pressure-vessel thickness increments require declared encodings or rounding; a continuous box alone does not define those mixed-variable instances. The formation study reports forty scenarios in a 30 m by 30 m workspace with ten obstacles and ten robots, a 20-coordinate decision vector, twelve inequalities and 60,000 evaluations per run. Assigning both a planar terminal slot and a planar approach waypoint to each robot would ordinarily require forty coordinates, so the reported encoding needs clarification. Complete pairwise clearances and obstacle checks also require an explicit constraint list; twelve inequalities cannot be assumed to enumerate all such checks. Dynamics, settling and collision feasibility remain unverified without the simulator and instance archive [3], [4–6].

The dispatch study reports fifteen units, one power-balance equality, twenty loads from 1,590 to 2,650 MW, twenty runs per load and 30,000 evaluations per run: 400 runs per method. Unit coefficients, capacity bounds, transmission-loss convention, equality normalization and tolerance are required to interpret its dollars-per-hour and MW outcomes [1], [2]. A reported residual is not by itself a certificate of feasibility. The moving-peaks study is described as ten peaks in five dimensions, height range 30–70, width range 12–15, shifts every 1,000 evaluations and sixty changes per run [43]. Severities are 1.0, 2.5 and 5.0, with 41 runs each. These settings require the original generator, moving-peak convention and reevaluation policy to identify one scalar offline-error observation per run.

5.2 | Reference Algorithms and Comparison Design

Fourteen baseline identities are specified: GA, DE, SHADE, L-SHADE, CMA-ES, PSO, Grey Wolf Optimizer (GWO), Whale Optimization Algorithm (WOA), Harris Hawks Optimization (HHO), Lion Optimizer (ALO), Artificial Bee Colony (ABC), Sine Cosine Algorithm (SCA), Salp Swarm Algorithm (SSA) and Water Cycle Algorithm (WCA) [27-36]. This is a broad comparison set, but its completeness or strongest published status is not established. Reference-code descent and unified safeguards require versioned implementations [37-47]. A common external penalty and ε wrapper is described for all methods. Such a wrapper changes acceptance relative to their original designs, so the comparison would concern wrapper-modified implementations. Matched tuning, initialization and evaluation work remain conditional on the counter and configuration ledgers; a common nominal budget does not certify equal computational effort.

GA supplies recombination and mutation, DE supplies difference-based trials, SHADE and L-SHADE supply history and population-size adaptation, CMA-ES adapts its sampling distribution, and PSO supplies velocity-based attraction [6], [8], [9]. The selected implementations can test different mechanisms, but no family serves as a universal upper bound on performance. ABC uses employed, onlooker and scout roles, with abandonment providing a restart mechanism. It is a relevant comparator to recovery-based search, although the reported outcomes do not isolate the causal value of each restart design. SCA uses sine and cosine position updates. Its scheduled amplitude differs from the reported entropy feedback, but relative accuracy or tuning insensitivity must be measured under declared conditions rather than inferred from that structural difference [44]. SSA uses leader–follower movement [45], and WCA uses ranked stream, river and sea relationships with restart operations [46]. These are relevant structural comparisons. A few reported task wins do not establish a universal constrained-engineering record or a mechanistic explanation of losses elsewhere.

5.3 | Run Protocol, Statistics, and Reproducibility

The described 41 runs per function give 492 runs per method and dimension across twelve functions. An odd sample count makes a sample median unambiguous; it does not make it generally unbiased. Mean, dispersion, median, success count and evaluations-to-target require distinct aggregation rules. A censored target count should specify whether the median includes failures recorded at the budget or excludes them. The source describes an aligned-rank-transform factorial analysis on run-level errors, with algorithm and function factors [48], and separate Holm families of fourteen DIS contrasts at each dimension [49]. *Eq. (17)* is the alignment expression for the algorithm effect in a balanced design. The actual model terms, dependence structure, alignment diagnostics and contrast procedure are required; ordinary pairwise tests on main-effect aligned ranks do not automatically inherit a valid factorial contrast analysis.

$$\tilde{Y}_{ijr}^{(A)} = Y_{ijr} - \bar{Y}_{\cdot j\cdot} - \left(\bar{Y}_{ij\cdot} - \bar{Y}_{i\cdot\cdot} - \bar{Y}_{\cdot j\cdot} + \bar{Y}_{\cdots} \ldots\right). \tag{17}$$

Wilson intervals [50] require an integer success count, a denominator and a binomial sampling interpretation; *Eq. (18)* supplies the corrected reporting formula. Pooling heterogeneous functions may describe a benchmark mixture, but independent common-probability Bernoulli sampling is an additional assumption. The source effect column matches signed win-minus-loss counts divided by all 24 cells in several rows, which is distinct from a paired signed-rank-biserial coefficient. Resampling should preserve function and dimension dependence [51].

$$\frac{\hat{p} + \frac{z^2}{2n} \pm z\sqrt{\frac{\hat{p}(1-\hat{p})}{n} + \frac{z^2}{4n^2}}}{1 + \frac{z^2}{n}}. \tag{18}$$

The source reports a composition-class fallback to Kruskal–Wallis and Dunn contrasts, with Holm adjustment. Skewness alone does not establish the required model or sampling assumptions. A fallback and

any preregistration claim require the original diagnostics, analysis code and timestamped protocol. Inferential labels below are retained as reported results pending that evidence [48]. The reported environment is a 3.2 GHz x86-64 core with 32 GB RAM and Python/NumPy. Timing per 10,000 evaluations measures a selected workload; it does not remove evaluation-cost differences. Original code, parameter files, seed lists, raw outputs and figure sources were not supplied for this analysis, so exact regeneration and public release are not asserted. Seed use is also described inconsistently as disjoint and identical in different sections; the original pairing ledger must resolve this.

6 | Results and Discussion

The results are interpreted as reported observations with explicit arithmetic and consistency checks. Several rankings differ across dimensions and task types, while unresolved interval, budget and aggregation issues prevent a blanket superiority or verified-significance conclusion.

6.1 | Benchmark Performance

The source reports a 28.7% mean relative improvement at 20D and a −6.8% margin at 40D. Computing a strongest-baseline-per-function reduction requires all twelve function rows for every baseline and an explicit rule for zero denominators. Only eight rows and three comparator columns are displayed in *Table 3*; the source also mentions two zero–zero exclusions while explicitly identifying only F1. The aggregate and its claimed equivalence to an L-SHADE-only comparison therefore remain unverified. The displayed F1 means for DIS and L-SHADE are zero, which does not certify exact attainment in every run without the error and rounding conventions. Other displayed rows show function-dependent differences. The source attributes them to scouts, coupling and cascade phases, but no intervention or diagnostic record establishes those mechanisms. *Table 3* shows five strict DIS mean wins, two L-SHADE mean wins and one displayed tie. On F7 the DIS/L-SHADE mean ratio is about 1.23, and on F12 about 1.20, rather than the source's 1.4 and 1.6 factors. These comparisons use the printed means only and do not establish paired statistical significance.

Table 3. Reported mean ± standard deviation of final error on eight selected CEC 2022 labels at 20D, described as 41 runs and 5,000d evaluations.

Function (Class)	DIS	L-SHADE	ABC	WCA
F1 (unimodal)	0.0 ± 0.0	0.0 ± 0.0	6.72e-9 ± 7.00e-9	1.08e-6 ± 2.03e-6
F2 (multimodal)	7.14e-10 ± 6.68e-10	1.16e-9 ± 7.49e-10	1.79e-8 ± 2.21e-8	3.87e-6 ± 5.98e-6
F4 (multimodal)	1.52e-9 ± 8.08e-10	2.60e-9 ± 2.57e-9	3.04e-8 ± 5.29e-8	4.44e-6 ± 6.42e-6
F6 (hybrid)	1.73e-9 ± 9.88e-10	4.45e-9 ± 5.08e-9	1.17e-6 ± 2.75e-6	4.50e-6 ± 5.95e-6
F7 (hybrid)	4.79e-9 ± 2.73e-9	3.89e-9 ± 2.73e-9	2.66e-6 ± 3.78e-6	2.18e-5 ± 4.71e-5
F8 (hybrid)	9.74e-9 ± 4.67e-9	1.46e-8 ± 1.16e-8	3.04e-6 ± 2.40e-6	3.53e-5 ± 5.16e-5
F10 (composition)	1.94e-6 ± 1.34e-6	3.18e-6 ± 2.25e-6	2.51e-4 ± 3.94e-4	1.93e-3 ± 2.31e-3
F12 (composition)	1.10e-5 ± 5.90e-6	9.16e-6 ± 7.22e-6	2.59e-3 ± 7.48e-3	0.0219 ± 0.0464

All numerical entries are preserved; function-version, counter and run-level records remain required. DIS has five strict mean wins and one displayed tie; L-SHADE has two strict mean wins. The reported mean-rank summary favors L-SHADE at 40D, with ranks 1.25 and 2.25 for L-SHADE and DIS. The full 40D function rows are absent, so eleven function wins and their mechanisms cannot be checked independently. Doubling dimension does not literally halve a defined search volume; that explanation requires a stated model and diagnostic evidence.

6.2 | Statistical Significance and Effect Sizes

The source reports ART algorithm statistics $F(14,7200) = 1025.6$ and 1178.1, and interaction statistics $F(154,7200) = 60.3$ and 77.9. These degrees of freedom are consistent with 180 balanced cells and 41 observations per cell, but the numerical test outputs cannot be verified from summaries. *Table 4* preserves the reported contrast values. A nondirectional F statistic does not itself establish the sign of a contrast; the source's assertion of thirteen favorable 40D contrasts also requires reconciliation with its four ABC losses described at that dimension.

Table 4. Reported ART contrast statistics, Holm-labeled p-values, source effect scores and win/tie/loss counts.

Baseline	F (20D)	Holm p (20D)	Holm p (40D)	Rank-Biserial [95% CI]	W/T/L
GAs	3995.7	0.0e+00	0.0e+00	+1.00 [+1.00, +1.00]	24/0/0
DE	238.6	1.7e-52	2.1e-34	+0.92 [+0.79, +1.00]	22/2/0
SHADE	130.2	1.3e-29	9.4e-15	+0.92 [+0.79, +1.00]	22/2/0
L-SHADE	8.6	3.4e-3	2.2e-10	-0.17 [-0.54, +0.21]	9/2/13
CMA-ES	3123.1	0.0e+00	0.0e+00	+0.92 [+0.79, +1.00]	22/2/0
PSO	2159.1	0.0e+00	1.2e-305	+1.00 [+1.00, +1.00]	24/0/0
GWO	1447.6	6.0e-288	5.0e-233	+1.00 [+1.00, +1.00]	24/0/0
WOA	4002.0	0.0e+00	0.0e+00	+1.00 [+1.00, +1.00]	24/0/0
HHO	1051.1	1.4e-214	1.8e-156	+1.00 [+1.00, +1.00]	24/0/0
ALO	4867.7	0.0e+00	0.0e+00	+1.00 [+1.00, +1.00]	24/0/0
ABC	504.1	2.3e-107	7.1e-67	+0.67 [+0.33, +0.92]	20/0/4
SCA	1840.8	0.0e+00	0.0e+00	+1.00 [+1.00, +1.00]	24/0/0
SSA	665.1	1.2e-139	4.5e-103	+1.00 [+1.00, +1.00]	24/0/0
WCA	2784.8	0.0e+00	0.0e+00	+1.00 [+1.00, +1.00]	24/0/0

Numerical entries are unchanged and inferential calculations remain unverified. Printed zero p-values denote a source numerical/reporting limit, not an exact probability of zero; each contrast direction requires its signed estimate. The reported effect values require a clarified estimator. For DE, SHADE and CMA-ES, 22 wins, two ties and no losses give $(22 - 0)/24 \approx 0.92$; excluding ties would give 1 for a signed-count effect, and a signed-rank effect would use ranked magnitudes. ABC's 20 wins and four losses give 0.67 with the all-cell denominator, while L-SHADE's nine wins and thirteen losses give −0.17. These arithmetic identities do not verify the labeled rank-biserial estimator or bootstrap intervals. *Table 4* contains nine +1.00 effect rows, including HHO and SSA, rather than the seven listed in the source prose. Ordinal dominance and interval-scale standardized differences answer different questions [53,54]. Neither an effect interval straddling zero nor a nonsignificant test establishes equivalence, and the reported all-cell scores should not be treated as a validated effect-size ladder. The source fallback reports $H(14) = 49.03$, $p = 8.9\times10^{-6}$, with $z = 2.02$ and 2.31 and Holm-labeled p-values 0.043 and 0.021. Conventional two-sided normal p-values for those z magnitudes are already approximately 0.0434 and 0.0209 before adjustment. The adjustment family, ordering and rounding must therefore be supplied; these values do not verify the claimed Holm procedure or confirm the ART inference.

Table 5. Reported mean ranks and success rates at the stated tolerance 10^−8, with historical interval entries preserved.

Method	Mean Rank 20D	Mean Rank 40D	Success 20D [CI]	Success 40D [CI]
DIS (proposed)	1.17	2.25	63.4% [61.1%, 65.5%]	8.3% [7.4%, 9.9%]
GAs	12.75	12.25	0.0% [0.2%, 0.6%]	0.0% [0.2%, 0.6%]
DE	3.83	4.58	8.9% [8.0%, 10.6%]	8.3% [7.4%, 9.9%]
SHADE	4.33	4.08	8.5% [7.6%, 10.1%]	8.3% [7.4%, 9.9%]
L-SHADE	2.00	1.25	60.6% [58.3%, 62.7%]	21.5% [19.9%, 23.6%]
CMA-ES	11.25	10.25	8.3% [7.4%, 9.9%]	8.3% [7.4%, 9.9%]
PSO	9.92	10.17	1.0% [0.9%, 1.9%]	0.0% [0.2%, 0.6%]
GWO	8.42	8.17	0.6% [0.6%, 1.4%]	0.0% [0.2%, 0.6%]
WOA	13.67	14.17	0.0% [0.2%, 0.6%]	0.0% [0.2%, 0.6%]
HHO	6.50	6.67	1.4% [1.2%, 2.4%]	0.6% [0.6%, 1.4%]
ALO	14.50	14.75	0.0% [0.2%, 0.6%]	0.0% [0.2%, 0.6%]
ABC	4.42	3.75	20.9% [19.3%, 23.0%]	14.6% [13.3%, 16.5%]
SCA	9.33	12.08	2.8% [2.4%, 4.0%]	0.4% [0.4%, 1.1%]
SSA	6.42	5.67	3.5% [3.0%, 4.7%]	0.8% [0.7%, 1.6%]
WCA	11.50	9.92	0.0% [0.2%, 0.6%]	0.0% [0.2%, 0.6%]

Table 5 preserves mean ranks and reported success percentages and intervals. Their stated denominator is 492. The printed intervals do not match conventional 95% Wilson intervals at that denominator: for example, zero successes would give lower endpoint zero and an upper endpoint about 0.775%, whereas several displayed zero-success intervals are [0.2%,0.6%]. The success point estimates remain descriptive source reports; their

integer counts, denominators and intervals need reconciliation. The intervals are not verified Wilson intervals for n = 492 and must be reconciled against original integer counts and sampling units; they are not used here for a confidence claim.

6.3 | Ablation Study

The four removal configurations are described as freezing topology, replacing influence with fitness-blind steps, fixing β, and replacing the ε/penalty/boundary machinery. They require matched counter traces and exact code branches to be interpreted as controlled interventions. The last variant changes multiple design choices, and a fixed initial nearest-neighbor graph is not necessarily an initial random graph.

Table 6 and *Fig. 1* show the largest displayed median gap for influence removal. Ratios to the full value 4.74×10^−8 are approximately 4.43×10^4, 1.57×10^4, 3.10×10^2 and 1.24×10^2 for influence, ε, rate and topology removal, respectively, consistent with the rounded table entries. Eleven one-direction differences give an unadjusted two-sided sign-test probability 2/2^11; a four-test Holm family can yield about 3.9×10^−3. This arithmetic possibility does not verify a signed-rank test or the original paired outputs. Numerical entries are preserved. The source alternates 'sign-test' and 'Wilcoxon' terminology; original paired differences and the test implementation are required to identify the actual procedure.

Table 6. Reported ablation median gaps, fold changes, mean ranks, Holm-labeled p-values and win/tie/loss counts.

Variant	Median Gap	Fold Change	Mean Rank	Holm p	W/T/L
DIS (full)	4.74e-8	1×	1.0	-	-
DIS-T (frozen topology)	5.88e-6	1.2e+2×	2.0	3.9e-3	11/0/0
DIS-β (fixed rate)	1.47e-5	3.1e+2×	3.0	3.9e-3	11/0/0
DIS-ε (static penalty)	7.42e-4	1.6e+4×	4.0	3.9e-3	11/0/0
DIS-I (no influence)	2.10e-3	4.4e+4×	5.0	3.9e-3	11/0/0

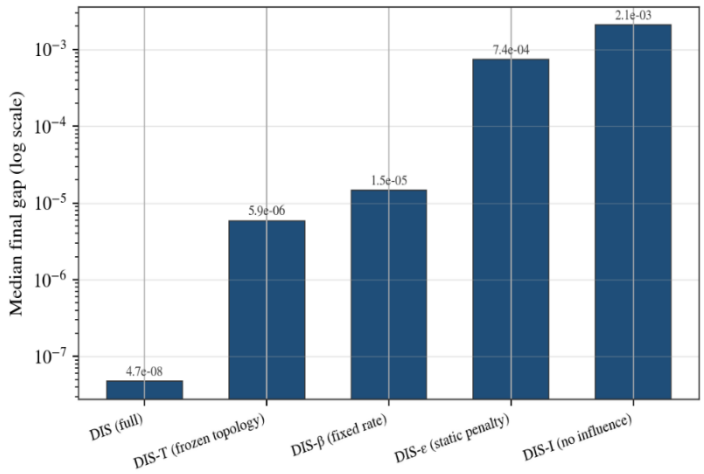


Fig. 1. Retained source plot of reported median gaps for the full and removal configurations.

Its displayed ordering agrees with *Table 6*. It does not show uncertainty, evaluation counters or isolate causal contributions of individual mechanisms. The removal ordering is consistent with an important role for the declared influence configuration in the reported study. It does not demonstrate that an epidemic mechanism, rather than all changed proposal and acceptance details, caused the difference. Claims about infeasible attractors likewise require residual trajectories and original code. The reported R sweep uses 1, 2, 5, 10 and 20 iterations, with small-gap values up to 4.2×10^−9 for R ≤ 5, 5.8×10^−9 for R = 10 and 2.6×10^−7 for R = 20; normalized weight entropy is reported to decline from 0.93 to 0.61 and distinct-neighbor counts from 38 to 3.1. These summaries are retained descriptively. Their aggregation differs from the full-ablation median 4.74×10^−8 and needs reconciliation. No causal cascade or optimal knee is verified from the sweep alone.

6.4 | Convergence Behavior

Fig. 2 shows a selected source trace through 2500 iterations. The prose reports a DIS terminal value near 4.5×10^−9 and labels the run median-selected, but *Table 3* reports a nonnegative F6 mean of 1.73×10^−9. For 41 nonnegative observations, their sample median cannot exceed (41/21) times their mean, about 3.38×10^−9 here, if both summaries use the same data and error definition. The trace's selection and aggregation are therefore unresolved. Its plotted early decline also does not display the claimed long dormant phase. The trace gives lower plotted DIS values than the other displayed methods after the initial point, while the source describes an early-above/late-below crossover on twenty cells. Linked per-run trajectories are required to verify that separate statement or attribute it to entropy and recovery. Error trajectories alone do not identify optimizer mechanisms.

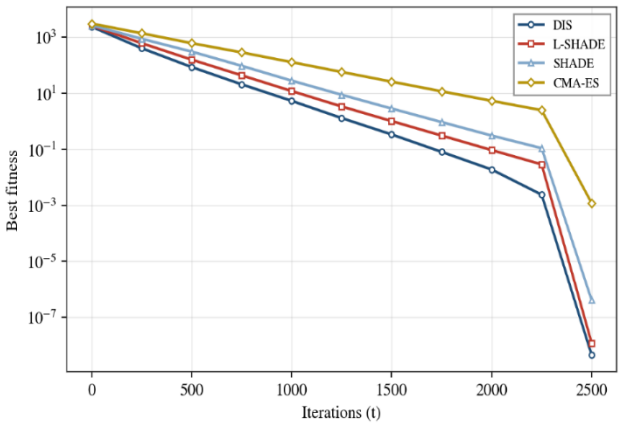


Fig. 2. Retained source best-fitness traces labeled F6 at 20D.

The 'median run' selection is unresolved against the reported F6 mean. At N = 60, 2500 full one-evaluation-per-agent iterations require 150,000 calls plus initialization, exceeding the stated 100,000-call budget. Original evaluation-counter traces must resolve the axis and budget before a matched-work comparison is asserted.

6.5 | Robustness and Scalability

The noise study reports independent multiplicative perturbations $\tilde{f} = f(1 + \xi)$ with standard deviations 0.01, 0.05, 0.10 and 0.20. DIS gap summaries are 4.2×10^−9, 6.8×10^−8, 9.2×10^−4 and 2.4×10^−2, versus 5.8×10^−6, 1.7×10^−5, 6.5×10^−3 and 3.4×10^−2 for L-SHADE. Those descriptive values are not verified noise-robustness effects without the run outputs and noiseless final-evaluation rule. Perturbing a biased raw CEC objective gives noise even at its biased optimum; a pairwise gate does not average independent noise merely by taking a score difference. *Fig. 3* and *Table 7* show threshold-count medians at 20, 40 and 80 dimensions. The printed three-point log–log slopes are approximately 1.25, 1.48 and 1.55, consistent with the retained exponent entries. Such slopes are descriptive fits to three reported medians, not an asymptotic scalability proof. Extension definitions, target censoring, initialization and counter conventions remain required. *Table 7* favors L-SHADE in terminal median gap at 40D: 2.99×10^−8 versus 3.20×10^−7 for DIS. At 80D the displayed DIS gap 2.61×10^−7 is slightly below L-SHADE's 2.74×10^−7, so the source claim that L-SHADE's terminal advantage persists at 80D is incorrect. These pooled medians do not identify per-function wins or statistical significance. Numerical entries are retained; 40D and 80D are custom extensions of the official CEC 2022 dimensional protocol. The exponent column is a three-point descriptive fit.

Table 7. Reported pooled median gaps and censored evaluations-to-target at 20, 40 and 80 dimensions.

Method	Gap 20D	Gap 40D	Gap 80D	Evals 20D	Evals 40D	Evals 80D	Exp.
DIS	3.12e-9	3.20e-7	2.61e-7	2.40e+4	5.60e+4	1.35e+5	1.25
L-SHADE	3.47e-9	2.99e-8	2.74e-7	3.20e+4	8.60e+4	2.50e+5	1.48
SHADE	4.50e-7	1.39e-5	5.73e-5	4.20e+4	1.20e+5	3.60e+5	1.55

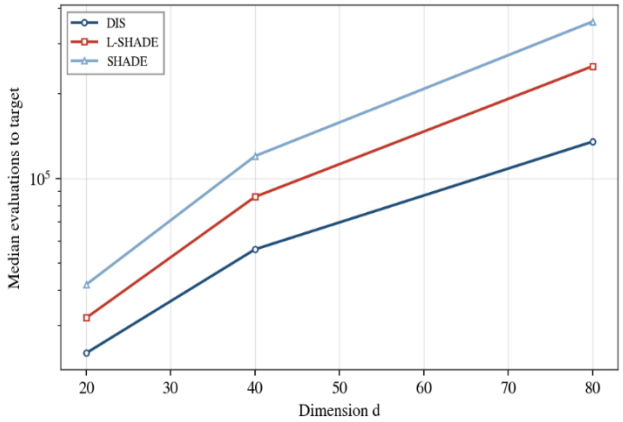


Fig. 3. Retained source threshold-count medians at three dimensions.

The 'median run' selection is unresolved against the reported F6 mean. The 'median run' selection is unresolved against the reported F6 mean. The reported slopes 1.25, 1.48 and 1.55 are consistent with the printed endpoints. They do not establish asymptotic complexity or equal timing, and the target/censoring and evaluation-count records remain unresolved.The source reports 11–14% topology overhead relative to L-SHADE, 21% lower median time-to-target on a multimodal subset, and less than 1% overhead in expensive-evaluation applications. These are separate timing statements with undocumented denominators, censoring and trace records. They remain reported observations rather than an independently validated accounting of end-to-end work.

6.6 | Reported Engineering Applications

The reported four-problem summaries favor WCA on welded beam, speed reducer and gear train, and DIS on pressure vessel. *Table 8* rounds several entries too coarsely to reconstruct the source's precise relative margins. The additional precise source means, 1.7249 for welded beam, 2994.5 for speed reducer and 5885.9 for DIS pressure vessel, require original outputs and feasibility records. The source list of five L-SHADE values for four problems is not adopted as a reconciled result.

Reported first-feasible counts are 312 ± 96 for DIS and 289 ± 84 for WCA on the engineering set, versus 1940 ± 520 for L-SHADE; formation counts are 580 ± 140, 640 ± 170 and 1090 ± 310, respectively. Mean and dispersion alone do not establish statistical indistinguishability or a causal delay from population reduction. Feasibility definitions and original scenario/run aggregation are required.

The source describes wrapper feasibility rates of 100% for DIS and WCA, 97.6% for L-SHADE, 95.1% for GA and 92.7% for ALO, and lower static-penalty rates of 82.9%, 76.5%, 61.0%, 53.7% and 41.5%. A reported mean terminal residual of 3.4×10^−3 and delays of 57–72% accompany that comparison. These values remain unreconciled reports without counts, normalization and tolerance rules; they do not establish that the ε rule caused each difference. The formation report gives DIS error 0.083 ± 0.011 m, ABC 0.102 ± 0.031 m, WCA 0.111 ± 0.026 m, L-SHADE 0.119 ± 0.028 m and PSO 0.151 ± 0.042 m. The printed DIS–L-SHADE mean reduction is about 30.3%; the DIS reduction relative to ABC, the lowest displayed rival, is about 18.6%. Two, three and four infeasible scenarios are reported for GA, SCA and ALO. DIS feasibility and the proposed trajectory explanation require the unresolved encoding, simulator and clearance archive.

The dispatch report gives DIS mean cost 31,842.6 ± 96.4 $/h, best single-run cost 31,706.2 $/h and mean balance residual 6.1×10^−4 MW; L-SHADE, WCA and DE means are 32,097.8, 32,143.5 and 32,410.2 $/h. The descriptive DIS reductions are about 0.8% and 1.8% against L-SHADE and DE, respectively, using the printed means. Fourteen DE and twenty-three SCA infeasible runs are reported. The claim that all 400 DIS runs are feasible is unresolved: The stated final ε of 10^−12 is not the reported physical residual tolerance unless a separate normalization and practical equality rule is supplied.

Table 8. Reported engineering and application summaries. Numerical entries are preserved.

Problem	d	m	Budget	Best	DIS	Best Rival
Welded beam	4	5	25,000	WCA	1.73 ± 1.10e-3	1.72 ± 2.00e-4
Pressure vessel	4	4	25,000	DIS	5.89e+03 ± 1.8	5.89e+03 ± 6.4
Speed reducer	7	11	25,000	WCA	3e+03 ± 0.21	2.99e+03 ± 0.03
Gear train	4	0	25,000	WCA	4.60e-11 ± 1.90e-10	2.70e-12 ± 9.30e-13
Robot formation	20	12	60,000	DIS	0.083 ± 0.011	0.102 ± 0.031
Economic dispatch	15	1	30,000	DIS	3.18e+4 ± 96.4	3.21e+4 ± 118

The 'Best rival' row for robot formation corresponds to ABC, while dispatch corresponds to L-SHADE; equality and inequality counts are not interchangeable. Instance equations, mixed-variable encodings, residual tolerances and run/scenario aggregation remain required before feasibility or deployment success is certified.

6.7 | Dynamic Environment Tracking on the Moving-Peaks Benchmark

The moving-peaks comparison reports 41 runs per severity and sixty changes per run. Offline error is described as one scalar over each run, and recovery as evaluations to regain 95% of pre-shift quality. A valid dynamic archive requires explicit reevaluation after a change; the metric also needs an objective convention, since a percentage of pre-shift quality need not be invariant to objective offsets. The reported paired Wilcoxon analysis pools 123 severity–run pairs per rival with a two-comparison Holm family [53]. *Table 9* reports DIS offline means 2.29, 2.35 and 2.51, versus L-SHADE 4.54, 5.07 and 5.43 and SHADE 5.30, 5.78 and 6.22. Printed DIS reductions against L-SHADE are approximately 49.6%, 53.6% and 53.8%; original unrounded values would be needed to recover the source's other rounded percentages. Recovery-count entries favor DIS descriptively. Reported adjusted p-values 7.3×10^−22 and 6.5×10^−22 and effect scores 0.97 and 0.98 cannot be verified without paired observations, tie handling and the effect definition.

Table 9. Reported moving-peaks offline error and recovery-count summaries, with all numerical entries preserved.

Severity	DIS Offline	L-SHADE Offline	SHADE Offline	DIS Recovery	L-SHADE Recovery	SHADE Recovery
1.0	2.29 ± 0.515	4.54 ± 0.937	5.3 ± 1.06	236 ± 31	512 ± 58	584 ± 62
2.5	2.35 ± 0.503	5.07 ± 1.12	5.78 ± 1.23	289 ± 36	604 ± 66	692 ± 71
5.0	2.51 ± 0.428	5.43 ± 1.17	6.22 ± 1.01	341 ± 42	701 ± 74	818 ± 83

Recovery is described as 95% of pre-shift quality. Original dynamic reevaluation, quality convention, pairing and analysis outputs are required; no verified paired significance or stability claim is inferred from these summaries.

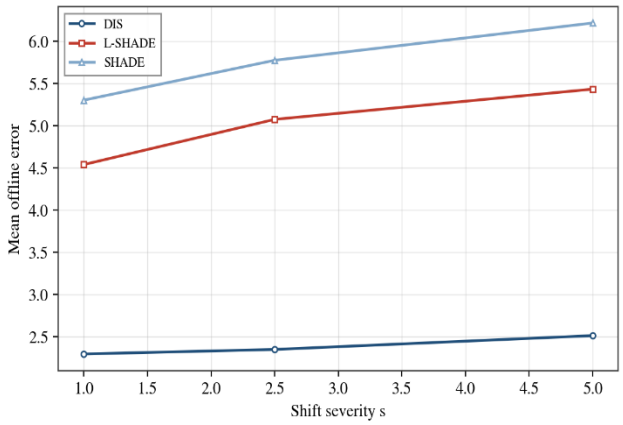


Fig. 4. Retained source offline-error means at three reported shift severities.

The displayed DIS reductions relative to L-SHADE are about 49.6%, 53.6% and 53.8%. The panel displays means without uncertainty and does not reveal change detection, archive reevaluation or recovery trajectories.

An environmental change can increase or decrease fitness-weight entropy; its direction is not fixed by the architecture. Recovery and neighbor rebuilding may assist tracking, but the proposed automatic dormant–cascade explanation needs entropy, β and event traces. Multiswarm designs provide related dynamic-search context [53], without validating the present causal explanation.

7 | Threats to Validity and Limitations

Internal validity is limited by missing original implementations, counter traces, tuning logs and seed pairing. The source alternates disjoint and identical seed-stream descriptions and claims alternative-seed reruns without providing outputs. Initialization, unbounded proposals, changing penalty scores and the *Fig. 2* iteration count need reconciliation before matched-budget or reproducibility claims are restored.

External validity is limited to the reported functions and application settings. The custom 40D/80D suite extensions, modified shared wrapper and mixed-variable engineering encodings require explicit definitions. A small application base cannot establish broad deployment performance, and the no-free-lunch theorem supplies no selected-problem superiority guarantee [13]. Dynamic constraints and equality-heavy changing problems remain untested here.

Construct validity depends on distinguishing objective error, feasibility, time-to-target, censored counts and runtime. Reported success intervals are inconsistent with the stated Wilson denominator, the effect label is ambiguous, and the F6 mean and selected trace conflict under a common nonnegative-error interpretation. Statistical comparison principles [53-56] require the original analysis records, rather than a visual agreement of ranks and plots. The source describes parameter sweeps, ±20% perturbations and variance-based screening [57], with calibration on ten held-out problems and 21 runs per configuration. Those records were not supplied. They remain protocol claims requiring the original problem list, tuning budget and outputs, rather than an established flat response surface. Nearest-neighbor maintenance and dynamic archive reevaluation are additional costs that a future validation must measure.

8 | Conclusion

DIS specifies fitness-gated neighborhood transfers, entropy feedback and recovery as a population-search design. The conditional coverage proposition identifies what a fixed-objective archive and proposal kernel would need for global convergence. It does not establish those conditions for the reported unrestricted, changing-score implementation. The retained numerical summaries show task- and dimension-dependent rankings, with unresolved inference, counter and feasibility records. The displayed results provide descriptive comparisons: several 20D rows favor DIS, the reported 40D ranks favor L-SHADE, WCA leads three of four engineering rows, and DIS has lower displayed formation, dispatch and moving-peaks means than the shown rivals. These observations motivate traceable validation of the design; they do not certify a universal advantage, an epidemic cause or practical feasibility. Further work should first release the original implementation, experiment manifest, run outputs, evaluation counters, timing records and figure sources. This would resolve the budget, aggregation, interval and feasibility conflicts before a new experiment is proposed. Learned edge weights could connect the design with adaptive pursuit and bandit credit assignment [34], [35]. Such an extension requires a declared reward and exploration rule; it is not an implemented result of this study.

Multiobjective and surrogate-assisted variants need explicit value, dominance and evaluation conventions. Their performance cannot be inferred from the current single-objective summaries. A decentralized implementation would require communication, asynchronous update and consistency protocols. Local centroid semantics alone do not demonstrate a working distributed robot-fleet system. Theory for the actual λ–ϵ schedule should distinguish objective minimization, feasible acceptance and archive memory. Noise and environmental shifts require their own evaluation and reevaluation arguments [18], [42]. Application validation must provide scenario generators, plant or robot models, unit-consistent residual scales, mixed-variable encodings and practical feasibility tolerances. Authors must confirm names, affiliations, ORCID

identifiers, funding, conflicts of interest and any assistance declarations before submission. Original code and data release remain pending confirmation; this revision supplies no author attestations. The present result is a corrected conditional analysis and a calibrated account of reported observations. Publication-level computational validation remains dependent on the original artifacts and reconciliation of the identified inconsistencies.

Conflict of Interest

The authors certify that they have no affiliations with or involvement in any organization or entity with any financial or non-financial interest in the subject matter discussed in this manuscript.

Data Availability

All data relevant to this study are contained within the manuscript. Additional information is available from the corresponding author upon reasonable request.

Funding

The authors received no financial support for the research, authorship, and/or publication of this article. This work was completed without external funding.

References

[1] Wood, A. J., & Wollenberg, B. F. (2003). *Power generation, operation, and control*. Wiley. https://www.wiley.com/en-us/shop/general-energy/power-generation-operation-and-control-3rd-edition-p-9780471790556

[2] Sinha, N., Chakrabarti, R., & Chattopadhyay, P. K. (2003). Evolutionary programming techniques for economic load dispatch. *IEEE transactions on evolutionary computation*, *7*(1), 83-94. https://doi.org/10.1109/tevc.2002.806788

[3] LaValle, S. M. (2006). *Planning algorithms* (Vol. 1). Cambridge, UK: Cambridge university press. https://doi.org/10.1017/CBO9780511546877

[4] Latombe, J. C. (1991). Potential field methods. In *Robot motion planning* (pp. 295-355). Boston, MA: Springer US. https://doi.org/10.1007/978-1-4615-4022-9

[5] Kavraki, L. E., Svestka, P., Latombe, J. C., & Overmars, M. H. (1996). Probabilistic roadmaps for path planning in high-dimensional configuration spaces. *IEEE transactions on robotics and automation*, *12*(4), 566-580. https://doi.org/10.1109/70.508439

[6] LaValle, S. M., & Kuffner Jr, J. J. (2001). Randomized kinodynamic planning. *The international journal of robotics research*, *20*(5), 378-400. https://doi.org/10.1177/02783640122067453

[7] Eiben, A. E., & Smith, J. E. (2003). *Introduction to evolutionary computing* (Vol. 53, p. 18). Berlin: springer. https://doi.org/10.1007/978-3-662-44874-8

[8] Tanabe, R., & Fukunaga, A. S. (2014). Improving the search performance of SHADE using linear population size reduction. In *2014 IEEE congress on evolutionary computation (CEC)* (pp. 1658-1665). IEEE. https://doi.org/10.1109/cec.2014.6900380

[9] Price, K. V., Storn, R. M., & Lampinen, J. A. (2005). *Differential evolution: A practical approach to global optimization*. Berlin, Heidelberg: Springer Berlin Heidelberg. https://doi.org/10.1007/3-540-31306-0

[10] Watts, D. J., & Strogatz, S. H. (1998). Collective dynamics of 'small-world'networks. *Nature*, *393*(6684), 440-442. https://doi.org/10.1038/30918

[11] Kermack, W. O., & McKendrick, A. G. (1927). A contribution to the mathematical theory of epidemics. *Proceedings of the royal society of London. Series A, Containing papers of a mathematical and physical character*, *115*(772), 700-721. https://doi.org/10.1098/rspa.1927.0118

[12] Pastor-Satorras, R., & Vespignani, A. (2001). Epidemic spreading in scale-free networks. *Physical review letters*, *86*(14), 3200. https://doi.org/10.1103/physrevlett.86.3200

[13] Wolpert, D. H., & Macready, W. G. (1997). No free lunch theorems for optimization. *IEEE transactions on evolutionary computation*, *1*(1), 67-82. https://doi.org/10.1109/4235.585893

[14] Coello, C. A. C. (2002). Theoretical and numerical constraint-handling techniques used with evolutionary algorithms: A survey of the state of the art. *Computer methods in applied mechanics and engineering*, *191*(11-12), 1245-1287. https://doi.org/10.1016/s0045-7825(01)00323-1

[15] Mezura-Montes, E., & Coello, C. A. C. (2011). Constraint-handling in nature-inspired numerical optimization: Past, present and future. *Swarm and evolutionary computation*, *1*(4), 173-194. https://doi.org/10.1016/j.swevo.2011.10.001

[16] Deb, K. (2000). An efficient constraint handling method for genetic algorithms. *Computer methods in applied mechanics and engineering*, *186*(2-4), 311-338. https://doi.org/10.1016/s0045-7825(99)00389-8

[17] Takahama, T., & Sakai, S. (2006). Constrained optimization by the ε constrained differential evolution with gradient-based mutation and feasible elites. In *proceedings of 2006 IEEE congress on evolutionary computation* (pp. 308-315). https://doi.org/10.1109/cec.2006.1688283

[18] Newman, M. E. J. (2002). Spread of epidemic disease on networks. *Physical review e, 66*(1), Article 016128. https://doi.org/10.1103/PhysRevE.66.016128

[19] Barabási, A., L. Albert, R. (1999). Emergence of scaling in random networks. *Science, 286*(5439), 509–512. https://doi.org/10.1126/science.286.5439.509

[20] Kumar, A., Price, K. V., Mohamed, A. W., Hadi, A. A., & Suganthan, P. N. (2021). *Problem definitions and evaluation criteria for the CEC 2022 special session and competition on single objective bound constrained numerical optimization*. https://raw.githubusercontent.com/P-N-Suganthan/2022-SO-BO/main/CEC2022%20TR.pdf

[21] Rogers, E. M., Singhal, A., & Quinlan, M. M. (2014). Diffusion of innovations. In *An integrated approach to communication theory and research* (pp. 432-448). Routledge. https://doi.org/10.1016/j.swevo.2011.10.001

[22] Granovetter, M. (1978). Threshold models of collective behavior. *American journal of sociology*, *83*(6), 1420-1443. https://doi.org/10.1086/226707

[23] Goldenberg, J., Libai, B., & Muller, E. (2001). Talk of the network: A complex systems look at the underlying process of word-of-mouth. *Marketing letters*, *12*(3), 211-223. https://doi.org/10.1023/a:1011122126881

[24] Kempe, D., Kleinberg, J., & Tardos, É. (2003, August). Maximizing the spread of influence through a social network. In *Proceedings of the ninth ACM SIGKDD international conference on Knowledge discovery and data mining* (pp. 137-146). Association for Computing Machinery. https://doi.org/10.1145/956750.956769

[25] Rudolph, G. (1994). Convergence analysis of canonical genetic algorithms. *IEEE transactions on neural networks*, *5*(1), 96-101. https://doi.org/10.1109/72.265964

[26] DeGroot, M. H. (1974). Reaching a consensus. *Journal of the American statistical association*, *69*(345), 118-121. https://doi.org/10.1080/01621459.1974.10480137

[27] Holland, J. H. (1992). *Adaptation in natural and artificial systems: An introductory analysis with applications to biology, control, and artificial intelligence*. The MIT press. https://doi.org/10.7551/mitpress/1090.001.0001

[28] Goldberg, D., E. (1989). *Genetic algorithms in search, optimization, and machine learning*. Addison-Wesley Longman Publishing Co., Inc.75 Arlington Street, Suite 300 Boston, MAUnited States. https://doi.org/10.5555/534133

[29] Kennedy, J., & Eberhart, R. (1995). Particle swarm optimization. In *Proceedings of ICNN'95-international conference on neural networks* (Vol. 4, pp. 1942-1948). IEEE. https://doi.org/10.1109/icnn.1995.488968

[30] Storn, R., & Price, K. (1997). Differential evolution–a simple and efficient heuristic for global optimization over continuous spaces. *Journal of global optimization*, *11*(4), 341-359. https://doi.org/10.1023/a:1008202821328

[31] Hansen, N., & Ostermeier, A. (2001). Completely derandomized self-adaptation in evolution strategies. *Evolutionary computation*, *9*(2), 159-195. https://doi.org/10.1162/106365601750190398

[32] Tanabe, R., & Fukunaga, A. (2013). Success-history based parameter adaptation for differential evolution. In *2013 IEEE congress on evolutionary computation* (pp. 71-78). IEEE. https://doi.org/10.1109/cec.2013.6557555

[33] Mirjalili, S., Mirjalili, S. M., & Lewis, A. (2014). Grey wolf optimizer. *Advances in engineering software*, *69*, 46-61. https://doi.org/10.1016/j.advengsoft.2013.12.007

[34] Mirjalili, S., & Lewis, A. (2016). The whale optimization algorithm. *Advances in engineering software*, *95*, 51-67. https://doi.org/10.1016/j.advengsoft.2016.01.008

[35] Heidari, A. A., Mirjalili, S., Faris, H., Aljarah, I., Mafarja, M., & Chen, H. (2019). Harris hawks optimization: Algorithm and applications. *Future generation computer systems*, *97*, 849-872. https://doi.org/10.1016/j.future.2019.02.028

[36] Bentley, J. L. (1975). Multidimensional binary search trees used for associative searching. *Communications of the ACM*, *18*(9), 509-517. https://doi.org/10.1016/j.advengsoft.2015.01.010

[37] Thierens, D. (2005). An adaptive pursuit strategy for allocating operator probabilities. In *Proceedings of the 7th annual conference on genetic and evolutionary computation* (pp. 1539-1546). Association for Computing Machinery. https://doi.org/10.1145/1068009.1068251

[38] DaCosta, L., Fialho, A., Schoenauer, M., & Sebag, M. (2008). Adaptive operator selection with dynamic multi-armed bandits. In *Proceedings of the 10th annual conference on Genetic and evolutionary computation* (pp. 913-920). Association for Computing Machinery. https://doi.org/10.1145/1389095.1389272

[39] Fialho, Á., Da Costa, L., Schoenauer, M., & Sebag, M. (2010). Analyzing bandit-based adaptive operator selection mechanisms. *Annals of mathematics and artificial intelligence*, *60*(1), 25-64. https://doi.org/10.1007/s10472-010-9213-y

[40] Karafotias, G., Hoogendoorn, M., & Eiben, Á. E. (2014). Parameter control in evolutionary algorithms: Trends and challenges. *IEEE transactions on evolutionary computation*, *19*(2), 167-187. https://doi.org/10.1109/tevc.2014.2308294

[41] Mallipeddi, R., & Suganthan, P. N. (2010). Problem definitions and evaluation criteria for the CEC 2010 competition on constrained real-parameter optimization. https://www.al-roomi.org/multimedia/CEC_Database/CEC2010/RealParameterOptimization/CEC2010_RealParameterOptimization_TechnicalReport.pdf

[42] Liang, J. J., Qu, B. Y., & Suganthan, P. N. (2013). Problem definitions and evaluation criteria for the CEC 2014 special session and competition on single objective real-parameter numerical optimization. http://bee22.com/manual/tf_images/Liang%20CEC2014.pdf

[43] Branke, J. (2002). *Evolutionary optimization in dynamic environments*. Dordrecht: Kluwer academic publishers. https://doi.org/10.1007/978-1-4615-0911-0

[44] Karaboga, D. (2005). *An idea based on honey bee swarm for numerical optimization*. https://abc.erciyes.edu.tr/pub/tr06_2005.pdf

[45] Mirjalili, S. (2016). SCA: A sine cosine algorithm for solving optimization problems. *Knowledge-based systems*, *96*, 120-133. https://doi.org/10.1016/j.knosys.2015.12.022

[46] Mirjalili, S., Gandomi, A. H., Mirjalili, S. Z., Saremi, S., Faris, H., & Mirjalili, S. M. (2017). Salp swarm algorithm: A bio-inspired optimizer for engineering design problems. *Advances in engineering software*, *114*, 163-191. https://doi.org/10.1016/j.advengsoft.2017.07.002

[47] Eskandar, H., Sadollah, A., Bahreininejad, A., & Hamdi, M. (2012). Water cycle algorithm–A novel metaheuristic optimization method for solving constrained engineering optimization problems. *Computers & structures*, *110*, 151-166. https://doi.org/10.1016/j.compstruc.2012.07.010

[48] Wobbrock, J. O., Findlater, L., Gergle, D., & Higgins, J. J. (2011). The aligned rank transform for nonparametric factorial analyses using only anova procedures. *Proceedings of the SIGCHI conference on human factors in computing systems* (pp. 143-146). Association for Computing Machinery. https://doi.org/10.1145/1978942.1978963

[49] Holm, S. (1979). A simple sequentially rejective multiple test procedure. *Scandinavian journal of statistics*, *6*(2), 65–70. https://scispace.com/pdf/a-simple-sequentially-rejective-multiple-test-procedure-458rh2uo9s.pdf

[50] Wilson, E. B. (1927). Probable inference, the law of succession, and statistical inference. *Journal of the American statistical association*, *22*(158), 209-212. https://doi.org/10.1080/01621459.1927.10502953

[51] Cliff, N. (1993). Dominance statistics: Ordinal analyses to answer ordinal questions. *Psychological bulletin*, *114*(3), 494. https://doi.org/10.1037/0033-2909.114.3.494

[52] Wilcoxon, F. (1945). Individual comparisons by ranking methods. *Biometrics bulletin*, *1*(6), 80–83. https://doi.org/10.2307/3001968

[53] Blackwell, T., & Branke, J. (2006). Multiswarms, exclusion, and anti-convergence in dynamic environments. *IEEE transactions on evolutionary computation*, *10*(4), 459-472. https://doi.org/10.1109/tevc.2005.857074

[54] García, S., Molina, D., Lozano, M., & Herrera, F. (2009). A study on the use of non-parametric tests for analyzing the evolutionary algorithms' behaviour: a case study on the CEC'2005 special session on real parameter optimization. *Journal of heuristics*, *15*(6), 617-644. https://doi.org/10.1007/s10732-008-9080-4

[55] Derrac, J., García, S., Molina, D., & Herrera, F. (2011). A practical tutorial on the use of nonparametric statistical tests as a methodology for comparing evolutionary and swarm intelligence algorithms. *Swarm and evolutionary computation*, *1*(1), 3-18. https://doi.org/10.1016/j.swevo.2011.02.002

[56] Friedman, M. (1937). The use of ranks to avoid the assumption of normality implicit in the analysis of variance. *Journal of the American statistical association*, *32*(200), 675-701. https://doi.org/10.1080/01621459.1937.10503522

[57] Saltelli, A., Annoni, P., Azzini, I., Campolongo, F., Ratto, M., & Tarantola, S. (2010). Variance based sensitivity analysis of model output. Design and estimator for the total sensitivity index. *Computer physics communications*, *181*(2), 259-270. https://doi.org/10.1016/j.cpc.2009.09.018